Impact of a Viscous Liquid Drop

Robert D. Schroll,[1] Christophe Josserand,[2] Stéphane Zaleski,[2] and Wendy W. Zhang[1]

[1]*Physics Department and the James Franck Institute, The University of Chicago, 929 East 57th Street, Chicago, Illinois 60637, USA*

[2]*UPMC Univ Paris 06, UMR 7190, Institut Jean Le Rond d'Alembert, F-75005 Paris, France and CNRS, UMR 7190, Institut Jean Le Rond d'Alembert, F-75005 Paris, France*

(Received 1 April 2009; published 21 January 2010)

We simulate the impact of a viscous liquid drop onto a smooth dry solid surface. As in experiments, when ambient air effects are negligible, impact flattens the falling drop without producing a splash. The no-slip boundary condition at the wall produces a boundary layer inside the liquid. Later, the flattening surface of the drop traces out the boundary layer. As a result, the eventual shape of the drop is a ''pancake'' of uniform thickness except at the rim, where surface tension effects are significant. The thickness of the pancake is simply the height where the drop surface first collides with the boundary layer.

DOI: 10.1103/PhysRevLett.104.034504 PACS numbers: 47.55.dr, 47.15.Cb

The impact of a liquid drop onto a dry solid surface lies at the heart of many important technological processes [1,2], from the application of a thermal spray [3–9] to fuel atomization [8,10–12]. Recently experiments revealed that the splash formed when a low-viscosity liquid, such as water or ethanol, hits a dry smooth wall at several m/s owes its existence entirely to the presence of air [13–18]. Reducing the ambient gas pressure eliminates the splash entirely. These results are motivating new studies on impact dynamics [19–28].

Here we reexamine the impact of a viscous liquid drop when air effects are absent. We use an axisymmetric volume-of-fluid (VOF) code to simulate the impact at reduced ambient pressure [29–32]. Our results are in quantitative agreement with experiments. They show that a boundary layer, corresponding to a thin region where the radial flow created by impact adjusts to the no-slip condition at the wall, is created by the impact. The boundary layer has uniform thickness. As impact nears its end, the drop surface flattens onto the boundary layer, evolving into a pancake of uniform thickness.

The simulation solves the Navier-Stokes equations, together with the constraint of incompressibility, for both the liquid interior and the gas exterior. The gas pressure, or equivalently the air density ρ_g, is kept so small that twofold changes in the value of ρ_g have little effect on the liquid dynamics. Across the drop surface, surface tension effects give rise to a Laplace pressure jump [29]. After impact onto the solid wall, the liquid flow inside the drop satisfies both the no-flux and no-slip boundary conditions at the solid wall. In the simulation, the bottom surface of the liquid drop is not broken upon impact. Finally, the entire system is enclosed in a cylindrical tube, as was done in the experiment. The only difference is that our simulation uses a tube of radius $R = 6a$ and height $H = 6a$, while the experiment uses a larger one. We have checked that results are unaffected by changes in the tube dimension.

Figure 1 plots successive drop surface shapes (outlined in white) calculated from a typical run of our simulation against snapshots from an experiment by Driscoll and Nagel under the same impact conditions [18]. This impact corresponds to a liquid drop of radius $a = 0.16$ cm hitting a dry smooth wall with speed $U_0 = 4$ m/s. The liquid is a low molecular weight silicone oil with dynamic viscosity $\mu_L = 9.4$ cP, density $\rho_L = 0.94$ g/cm^3, and surface tension $\sigma = 21$ dynes/cm. The exterior fluid corresponds to air at 34 kPa, with density $\rho_g = 4.4 \times 10^{-4}$ g/cm^3 and dynamic viscosity $\mu_g = 1.8 \times 10^{-2}$ cP. The comparison in Fig. 1 shows that the shape evolution calculated from the simulation agrees very well with the experiment. After the drop hits the wall, the liquid inside the drop is diverted outwards and expands radially along the wall [Fig. 1(b)]. Later, the falling drop flattens, evolving towards a shape resembling a pancake with a thickened outer rim [Fig. 1(c)]. By $t = 7.4\tau$, where $\tau \equiv a/U_0$ is a typical fall time for the drop, the expanding drop attains its maximum extent [Fig. 1(d)]. After that point in time, surface tension causes the drop in the simulation to retract inwards and reform into a spherical shape, a dynamics we do not analyze.

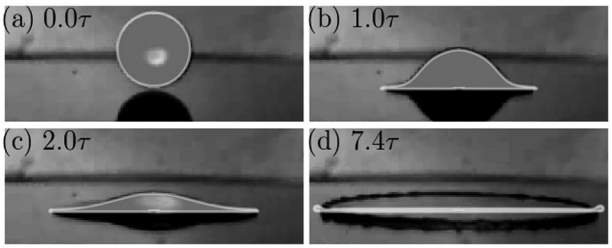

FIG. 1. Impact of a viscous silicone oil drop at 4 m/s onto a smooth, dry substrate at reduced ambient pressure (34 kPa). Surface profiles (white) from simulated impact are overlaid against snap shots from an experiment. From left to right, the successive times are $t = 0$, τ, 2τ and 7.4τ where $\tau \equiv a/U_0$ is the impact time scale. Here Re $\approx$ 1280 and We $\approx$ 2280.

In the rest of the Letter we examine how the formation of the pancake is controlled by the kinematics of impact, i.e., the drop radius and impact speed, as well as the material properties. To correlate outcomes from different impacts, we nondimensionalize the length scales by a, the velocities by U_0, and the time scales by τ. Since neither the tube dimensions nor the air properties affect the liquid dynamics reported here, the outcomes depend on only two dimensionless parameters: the Reynolds number $\mathrm{Re} \equiv 2\rho_L U_0 a/\mu_L$ and the Weber number $\mathrm{We} \equiv 2\rho_L U_0^2 a/\sigma$. The impact in Fig. 1 corresponds to $\mathrm{Re} \approx 1280$ and $\mathrm{We} \approx 2280$, within the viscous regime identified in [33].

Previous studies [33,34] proposed a simple estimate for the eventual thickness h of the pancake. The idea is that the only mechanism that can arrest the outward radial expansion is viscous dissipation. We then assume that the impact energy is dissipated by a radial flow of strength U_0 in a liquid pancake of thickness h and maximal extent $R_{\max}$. Balancing the dissipation against the initial kinetic energy yields

$$\frac{\mu_L U_0}{h}(\pi R_{\max}^2) R_{\max} \approx \frac{\rho_L U_0^2}{2}\left(\frac{4\pi a^3}{3}\right). \tag{1}$$

This energy balance, together with volume conservation $4\pi a^3/3 \approx \pi R_{\max}^2 h$, predicts that the dimensionless pancake thickness h/a should scale as $\mathrm{Re}^{-2/5}$. However, it does not tell us when the characteristic pancake thickness h first emerges. Nor does it explain why the drop would flatten into a sheet with such uniform thickness. Next we show that an understanding of the boundary layer formed upon impact provides natural explanations for both features. Very recently Roisman *et al.* studied the impact formed when a viscous drop hits a solid sphere using theory, experiment, and simulation [27,28]. This theoretical analysis also suggests that a boundary layer is present. However, no direct calculation of the vorticity distribution from the simulation, or its connection to the formation of the pancake structure in the experiment, were presented. These are the features we focus on next.

During the first instants of impact, when $t < t_{\max}$, the maximal radial extent of the liquid drop expands approximately as $\sqrt{4aU_0 t}$, quantitatively consistent with measurements from the experiment [35]. Thus the outermost edge of the "splat" formed upon impact both expands quickly and decelerates rapidly. To track its local evolution, we switch to a reference frame $x = r - R_h(t)$, where R_h is defined as a radial position directly behind the rim, instead of the cylindrical coordinate where the r axis is along the drop center line and $z = 0$. We then plot the calculated drop surface profiles within the new reference frame which is expanding outwards at approximately the same rate as the outermost edge [Fig. 2(a)]. We find that, initially ($t = 0.3\tau$) a thin collar is ejected from a nearly spherical drop. As time goes on, surface tension slows the edge of the expanding liquid sheet, causing liquid to accumulate into a rounded rim. This trend is consistent with results from previous studies [36–38]. This rounding of the outer rim also creates a local minimum in the height profile. To the left of the minimum (smaller radial distance from the center), the height slopes downwards. As time goes on, the downward slope becomes more and more gently sloped and the height flattens inwards. By $t = 4.9\tau$, a pancake of uniform thickness is apparent. In short, viewing the impact in this comoving reference frame reveals that the formation of the pancake proceeds in a simple way. A characteristic thickness h is first attained near the outermost rim, then propagates inwards without change.

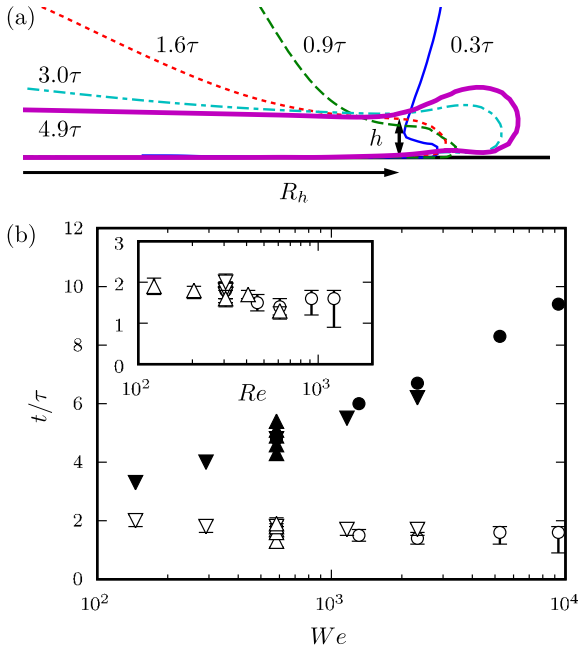

FIG. 2 (color online). Time evolution of the liquid sheet ejected after impact. (a) Shape evolution in the comoving frame $x = r - R_h(t)$ where $R_h(t) \approx 1.3\sqrt{U_0 a t}$. The impact speed $U_0 = 2$ m/s and the liquid viscosity $\mu_L = 0.2$ poise. Other parameters unchanged from that for Fig. 1. (b) Onset time t_{onset} (open symbols) and $t_{\max}$, the time of maximum radial extent (closed symbols) as a function of We. The different symbols correspond to different simulated impacts $U_0 =$ 2–8 m/s (○), $\sigma = 5.25$–84 dynes/cm (▽), and $\mu =$ 10–50 cP (△). Inset plots onset time t_{onset} vs Re.

From the simulation, we can quantify this dynamics by associating the first appearance of h with an onset time t_{onset}. Figure 2(b) plots t_{onset} as a function of the impact parameters. Nondimensionalizing t_{onset} by the impact time scale $\tau = a/U_0$ produces essentially flat curves with respect to both Re and We. This suggests that t_{onset} is primarily controlled by the kinematics of impact, with no strong dependence on either the liquid viscosity or surface tension. Moreover, within the range of impact examined, the onset time scale t_{onset} is always considerably shorter than $t_{\max}$, the time when the radial expansion produced by impact is halted and the drop retracts back to a nearly spherical shape. This suggests that the emergence of h is

not related to whether the kinetic energy has been sufficiently dissipated, but instead controlled by the fall time τ, which tells us how quickly the downward falling liquid drop comes into contact with the wall.

One feature which is strongly affected by the fall time is the generation and diffusion of vorticity within the liquid drop. Prior to impact, the drop is falling with a spatially uniform downward velocity and the vorticity is 0 everywhere inside the drop. After impact, the no-flux condition at the wall causes the liquid previously falling downwards to be diverted into a radially expanding flow. This expansion flow speeds up as it moves away from the center line, reaches a peak at R_h, then slows down as it enters the rim. This radial expansion also adjusts, via viscous effects, to the no-slip boundary condition at the solid wall. As a result of this adjustment, vorticity is generated in the liquid layer nearest to the solid wall. At any moment, the amount of vorticity generated to ensure zero slip at the wall is dictated by the strength of the radial expansion flow. Because the simulated impact is axisymmetric, only the azimuthal component of the vorticity is nonzero, i.e., $\boldsymbol{\omega} = \omega(r, z, t)\mathbf{e}_\theta$ where $\omega \equiv \partial u_z/\partial r - \partial u_r/\partial z$. For high Reynolds number flows this adjustment takes place inside a narrow boundary layer. In Fig. 3(a) we plot the wall value of the vorticity $\omega_0(r, t)$ [39]. Since the radial outflow is largest near the outer edge, the vorticity also has a maximum near R_h. As the impact proceeds, the downward fall of the liquid drop slows, retarding the expansion and thus reducing the magnitude of ω_0.

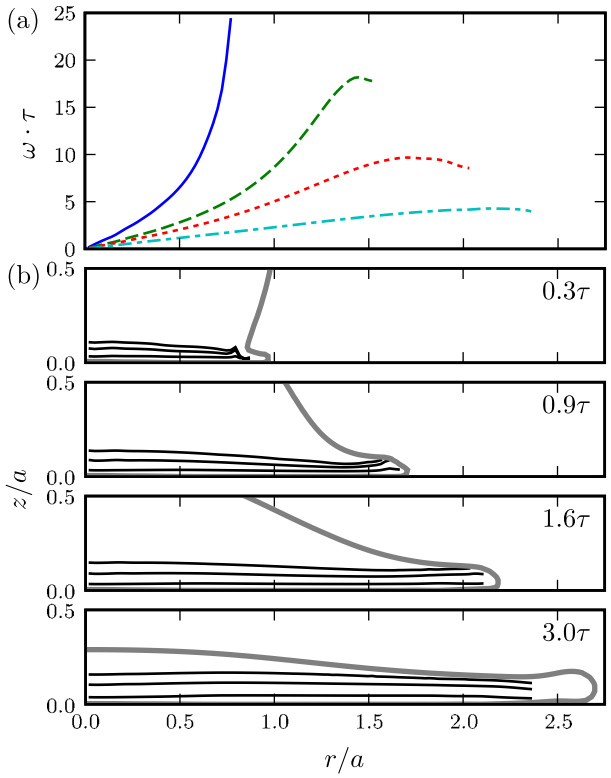

FIG. 3 (color online). Vorticity evolution after impact. (a) Value of the vorticity at the wall as a function of radial distance r [39]. From top to bottom, the profiles are taken at $t = 0.3\tau$, 0.9τ, 1.6τ, and 3.0τ. (b) The 20%, 50%, and 90% contours of the vorticity distribution.

We would like to delineate the spatial extent of the boundary layer from the spatial structure of the velocity field within the liquid drop. Our task is complicated by the fact that the absolute size of the vorticity is strongly correlated with the strength of the radial expansion flow. Since the radial expansion flow varies with r, vorticity is generated at different rates at different spatial locations. Moreover, at a given location, the vorticity production rate slows over time because the radial expansion slows. Thus contours of absolute vorticity do not provide clear indications for the spatial extent of the boundary layer. We sidestep this complication by normalizing $\omega(r, z, t)$, the vorticity distribution in the bulk of the liquid, by the "wall" value $\omega_0(r, t)$. This essentially strips away variations in the vorticity distribution due to the varying speed of the radial expansion flow. For simple high Reynolds number flows, such as a uniform flow past a solid wall, as well as the boundary layer created by a straining flow towards a solid wall [40], this procedure correctly reproduces the boundary layer structure that emerges from asymptotic analysis. In Fig. 3(b) we plot contours of the normalized vorticity distribution. In each snapshot, the solid lines within the liquid drop correspond to contours where $\omega(r, z, t)/\omega_0(r, t) = 90\%$ (lowest curve), 50%, and 20% (highest curve). At early times ($t = 0.3\tau$), the boundary layer delineated by the contours is a pancake-shaped region inside the liquid drop. Except at the outermost edge, the top surface of the liquid drop is widely separated from the boundary layer. As impact proceeds, the boundary layer extends radially and thickens slightly, but retains its pancake shape. At $t = t_{\text{onset}}$, the top surface of the drop collides with the boundary layer. After the collision, the surface at the collision location ceases to decrease in height. At the same time, the rest of the drop surface continues to fall downwards, bringing more and more portions of the surface into collision with the boundary layer. The result is a "front" that flattens inwards radially, tracing out the pancake-shaped boundary layer.

The idea that the eventual pancake thickness h first emerges when the top surface of the drop collides with the boundary layer suggests the following scaling relation for the eventual thickness h: If the boundary layer thickens diffusively prior to its collision with the top surface, then h would scale be approximately $\sqrt{\nu_L t_{\text{onset}}}$ where ν_L is the kinematic viscosity of the liquid. If t_{onset} is simply a/U_0 which is the simplest estimate suggested by Fig. 2, then h/a, the ratio of the pancake thickness to the drop radius follows the Blasius scaling $\text{Re}^{-1/2}$. If instead t_{onset} has a weak $\text{Re}^{1/5}$ variation, which is also consistent with our data, then $h/a \propto \text{Re}^{-2/5}$, reproducing the scaling law proposed previously. What is significant about the new scenario outlined here is not that it changes the scaling exponent for h/a, but that it provides a natural explanation

for why the characteristic pancake thickness first emerges near the rim, and also why the final shape is such a high degree of spatial uniformity. Both features are dictated by the structure of the viscous boundary layer.

Before concluding, we comment on how the boundary layer may affect splash formation. Air has negligible effects on the impact we simulate here. However, as t approaches 2τ, the radial expansion slows and the pressure gradient within the liquid sheet is essentially zero. In this time window, the boundary layer is not securely attached to the wall. Any external perturbation that adds an adverse pressure gradient, e.g., resistance from the air flow, can potentially cause the boundary layer to separate from the wall. Since the shape of the impacting drop at its outermost extent is coupled to the contours of the viscous boundary layer, the separating boundary layer may peel the thin liquid layer away from the wall, forming the beginning of a corona. Simulations to check this idea are under way [35].

In conclusion, we have simulated the impact of a viscous oil drop when the ambient air has negligible effects. Results on the large-scale shape deformation agree quantitatively with measurements from available experiments. The thin, spatially uniform pancake shape that a falling drop gets flattened into owes its existence to the boundary layer in the liquid drop created by impact.

The authors are grateful to Cacey Stevens, Michelle Driscoll, and Sidney Nagel for helpful discussions and for sharing unpublished data from their experiments. We thank Leo Kadanoff, Margo Levine, Alex Obakov, David Quéré, and Tom Witten for encouragement and helpful comments. This work was supported by the Keck initiative for ultrafast imaging and the Sloan Foundation (W. W. Z.). The photos in Fig. 1 are courtesy of M. Driscoll and S. R. Nagel.

[1] M. Rein, Fluid Dyn. Res. **12**, 61 (1993).
[2] A. L. Yarin, Annu. Rev. Fluid Mech. **38**, 159 (2006).
[3] H. Herman, S. Sampath, and R. McCune, MRS Bull. **25**, 17 (2000).
[4] X. Jiang, Y. Wan, H. Herman, and S. Sampath, Thin Solid Films **385**, 132 (2001).
[5] P. Fauchais, M. Fukumoto, A. Vardelle, and M. Vardelle, J. Therm. Spray Technol. **13**, 337 (2004).
[6] C. J. Li and J. L. Li, Surf. Coat. Technol. **184**, 13 (2004).
[7] A. McDonald, C. Moreau, and S. Chandra, Surf. Coat. Technol. **202**, 23 (2007).
[8] A. S. Molta and A. L. N. Moreira, Int. J. Heat Fluid Flow **28**, 735 (2007).
[9] K. Shinoda, H. Murakami, S. Kuroda, S. Oki, K. Takehara, and T. G. Etoh, Appl. Phys. Lett. **90**, 194103 (2007).
[10] F. A. Williams, Phys. Fluids **1**, 541 (1958).
[11] N. A. Chigier, Prog. Energy Combust. Sci. **2**, 97 (1976).
[12] A. H. Lefebvre, *Atomization and Sprays* (Hemisphere Publishing, New York, 1989).
[13] L. Xu, W. W. Zhang, and S. R. Nagel, Phys. Rev. Lett. **94**, 184505 (2005).
[14] D. Quéré, Nature (London) **435**, 1168 (2005).
[15] L. Xu, L. Barcos, and S. R. Nagel, Phys. Rev. E **76**, 066311 (2007).
[16] L. Xu, Phys. Rev. E **75**, 056316 (2007).
[17] C. Stevens, N. Keim, W. W. Zhang, and S. R. Nagel, in *Proceedings of the APS Division of Fluid Dynamics Meeting, 2007* (Report No. FC.00003).
[18] M. Driscoll, C. Stevens, and S. R. Nagel, in *Proceedings of the APS Division of Fluid Dynamics Meeting, 2008* (Report No. AG.00005).
[19] R. A. Jepsen, S. S. Yoon, and B. Demosthenous, Atom. Sprays **16**, 981 (2006).
[20] C. Duez, C. Ybert, C. Clanet, and L. Bocquet, Nature Phys. **3**, 180 (2007).
[21] S. Mukherjee and J. Abraham, J. Colloid Interface Sci. **312**, 341 (2007).
[22] H. J. Subramani, T. Al-Housseiny, A. U. Chen, M. Li, and O. A. Basaran, Ind. Eng. Chem. Res. **46**, 6105 (2007).
[23] R. D. Deegan, P. Brunet, and J. Eggers, Nonlinearity **21**, C1 (2008).
[24] R. Kannan and D. Sivakumar, Colloids Surf. A **317**, 694 (2008).
[25] R. E. Pepper, L. Courbin, and H. A. Stone, Phys. Fluids **20**, 082103 (2008).
[26] A. Mongruel, V. Daru, F. Feuillebois, and S. Tabakova, Phys. Fluids **21**, 032101 (2009).
[27] I. V. Roisman, E. Berberović, and C. Tropea, Phys. Fluids **21**, 052103 (2009).
[28] I. V. Roisman, Phys. Fluids **21**, 052104 (2009).
[29] B. Lafaurie, C. Nardone, R. Scardovelli, S. Zaleski, and G. Zanetti, J. Comput. Phys. **113**, 134 (1994).
[30] C. Josserand and S. Zaleski, Phys. Fluids **15**, 1650 (2003).
[31] C. Josserand, L. Lemoyne, R. Troeger, and S. Zaleski, J. Fluid Mech. **524**, 47 (2005).
[32] A review of several other volume-of-fluid simulations of drop impact is given in P. R. Gunjal, V. V. Ranade, and R. V. Chaudhari, AIChE J. **51**, 59 (2005).
[33] C. Clanet, C. Béguin, D. Richard, and D. Quéré, J. Fluid Mech. **517**, 199 (2004).
[34] S. Chandra and C. T. Avedisian, Proc. R. Soc. A **432**, 13 (1991).
[35] R. D. Schroll, Ph.D. thesis, University of Chicago, 2009.
[36] J. B. Keller, A. King, and L. Ting, Phys. Fluids **7**, 226 (1995).
[37] P. G. deGennes, D. Quéré, F. Brochard-Wyart, and A. Reisinger, *Capillary and Wetting Phenomena* (Springer-Verlag, Berlin, 2003).
[38] A. I. Fedorchenko, A. B. Wang, and Y. Wang, Phys. Fluids **17**, 093104 (2005).
[39] Since the bottom surface of the drop is not broken by impact, no liquid is ever in direct contact with the wall. We therefore define the wall value by taking the derivatives near the bottom surface at a fixed vertical height. Here we chose $z/a = 1/60$. Choosing different values makes no difference provided the vertical height is suitably small.
[40] D. J. Acheson, *Elementary Fluid Dynamics* (Clarendon Press, Oxford, 1990).